RESEARCH ARTICLE

European Journal of
Lipid Science and Technology
www.ejlst.com

A Configurational Approach to Model Triglyceride Pure Component Properties

Julia Seilert and Eckhard Flöter*

In this contribution, a new model to predict the thermodynamic properties, namely enthalpy of fusion (ΔH_f) and melting temperature (T_m), of pure triglycerides (TAGs) is presented. Different contributions to these properties could be expressed by means of repetitive structural attributes deduced from molecular structures. Carefully formulated configurational and geometrical simplifications enabled to attribute physical meaning to most of the parameters. Overall, the number of adjustable parameters is successfully minimized to less than half compared to the well-known model proposed by Wesdorp in "Liquid-multiple solid phase equilibria in fats: theory and experiments" (1990). Comparing both models revealed that the new model surpasses the reference model considering desirable prediction quality, thermodynamical consistency, and the number of adjustable parameters. ***Practical application*****: The successful description of the phase behavior of TAG mixtures is crucial to understand complex phenomena in fat-based products. This objective is based on reliable predictions of pure component properties and non-ideal mixing in liquid- and solid-phases. The newly formulated model gives reliable descriptions of experimental data and predictions of unknown data of TAGs — both thermodynamically consistent. Those are of benefit as prerequisite for any meaningful effort to predict the solid-liquid phase behavior of TAG mixtures as well as crystallization kinetics.**

1. Introduction

Understanding the phase behavior of fats is of importance in the spreads and confectionary industry. The solid fat content (SFC) in a product, fat crystal sizes, and their distribution are common characteristics of interest. These determine the mouthfeel of the product as well as the melting range and the solidification kinetics.[1] To reduce the number of experimental studies on this matter, mathematical modeling offers a valuable extension to predict these properties based on the solid-liquid phase behavior of triglycerides (triacylglycerols, short: TAGs). Several studies in this regard were performed over the course of the last decades.[2–6]

Usually, pure component data, namely enthalpy of fusion (ΔH_f) and melting temperature (T_m), of the respective TAGs composing the mixtures and mathematical models for non-ideal mixing in the liquid and solid phase are used for the prediction of the solid-liquid phase equilibria. A few models for predicting pure component properties[6–10] and the thermodynamic properties of mixtures[5,11–13] have been introduced.

Although TAGs are chemically very similar to each other, small changes in their chemical structure, for example, degree of saturation, chain length differences, glycerol backbone (GLY) configuration, affect the solid-liquid phase equilibria. It is generally acknowledged that the comprehensive description of the physical properties of TAGs is difficult. This challenge is further complicated by the fact that TAGs occur in different polymorphic forms. Even though TAG polymorphism is monotropic, that is, only one polymorph is stable over the entire temperature range, the so-called α, β', and β-polymorphs[14] are the most commonly considered. These three polymorphs differ in the hydrocarbon chain packing, their orientation (subcell), and the angle of tilt with respect to the lamellar interface. However, TAGs occur only in theory in all three polymorphic forms, β-polymorph being the most stable form. Further, TAGs arrange in at least two kinds of layered crystal stacking structures, that is, double chain length (DCL) and triple chain length (TCL).[15] This is due to lateral interactions (INTs) between hydrocarbon chains.

The GLY is believed to assume two configurations, namely tuning fork and chair. Which configuration the TAG assumes depends on the mix of fatty acids and their distribution on the glycerol backbone.

The aforementioned lamellar interface is characterized by the methyl end plane (MEP) formed by the terminal methyl groups of the fatty acid moieties. Its characteristics depend on the chain length mismatches (CLM) of hydrocarbon chains and the chain inclination of the respective polymorph. Assuming an

J. Seilert, Prof. E. Flöter
Department of Food Process Engineering
Technical University Berlin
Seestr. 13, 13353 Berlin, Germany
E-mail: julia.seilert@tu-berlin.de

The ORCID identification number(s) for the author(s) of this article can be found under https://doi.org/10.1002/ejlt.202100010

DOI: 10.1002/ejlt.202100010

even lamellar interface, differences in the chain lengths of adjacent fatty acids cause a disrupted interface. The resulting voids decrease the local crystal density.[16]

The described characteristics of TAGs are determined by various experimental methodologies such as differential scanning calorimetry (DSC) (ΔH_f and T_m) and X-ray diffraction (XRD) techniques (short spacing (SS), long spacing (LS), GLY configuration). Regarding modeling based on experimental data, the quality of the respective experimental data must be considered. Not only the availability of comprehensive data but also their quality are cornerstones for the formulation of reliable models. Besides plain experimental and methodological errors, uncertainties about the chemical composition and sample purity can compromise the starting point and verification options of any modeling effort. As a temperature-dependent measurement technique, the resulting thermograms of DSC analysis are greatly influenced by crystallization kinetics. In powder XRD measurements, samples comprising numerous crystals are measured. Hence, XRD reveals essentially only qualitative information on the subcell geometry (polymorph, obtained from SS in wide-angle spectra) and chain length stacking (LS in small-angle spectra).

TAG polymorphism is not limited to the named three structures, considering the six structures necessary to characterize the crystallization behavior of cocoa butter and other submodifications of unsaturated TAGs, for example, sub-α, δ, γ, β-1, β-2.[17–21] This adds uncertainty to experimental data.

In the well-established model by Wesdorp,[6] the TAG properties in three polymorphs are estimated based on the geometry of the TAG. Detailed information on the model can be found elsewhere.[6,22,23] Different configurations of the GLY, as well as different crystal structures, are not accounted for. The model predicts the properties of completely saturated and partially unsaturated TAGs. For the latter, the model requires a large number of parameters. Two approaches are used to predict T_m. In the first, T_m is approximated by a polynomial equation lacking any physical justification. In the second approach, T_m is calculated from the ratio of ΔH_f and entropy of fusion (ΔS_f) at thermodynamic equilibrium and respective ΔS_f equations. However, for either way it was pointed out that, in particular, sequences of predicted T_m partly lack thermodynamic consistency.[22]

A Group Contribution model by Zéberg-Mikkelsen et al.[7] emerges from UNIQUAC and is based on the interactions between the fatty acid moieties. The model describes, using a large parameter set, only the properties of saturated TAGs.

In this contribution, a new model to predict the pure TAG properties (ΔH_f and T_m) is described. Model equations were developed based on the configuration of the TAG in the crystal. Therefore, repetitive structural elements were derived from TAG analysis of known crystal structures. This corresponds to the ambition that model parameters represent recognizable contributions. Furthermore, the model fit is constrained to deliver thermodynamically consistent predictions.

2. Model Development

2.1. Notation

In this contribution, the TAGs are decoded by a three-letter code for convenience. For example, tripalmitin is decoded by PPP, where the middle character indicates the fatty acid on the 2-position of the glycerol backbone. The common denotation of selected fatty acids occurring in vegetable fats and oils is given in **Table 1**.

Table 1. Fatty acid nomenclature.

Fatty acid	Symbol	C:U
Capric acid	C	10:0
Lauric acid	L	12:0
Myristic acid	M	14:0
Palmitic acid	P	16:0
Stearic acid	S	18:0
Elaidic acid	E	18:1t
Oleic acid	O	18:1
Linoleic acid	l	18:2
Linolenic acid	le	18:3

The notation is given as *C:U* ("*C*" = carbon number, "*U*" = number of double bonds); "*t*" indicates a double bond in *trans*-configuration, if not indicated otherwise the double bonds are in *cis*-configuration.

Table 2. Number of available data on enthalpy of fusion (ΔH_f) and melting temperature (T_m) of TAGs in dataset *D*; data sorted after assigned crystal structures, DCL—double chain length stacking, TCL—triple chain length stacking; see text for details.

	α		β'		β	
	DCL	TCL	DCL	TCL	DCL	TCL
ΔH_f						
Saturated	44	15	30	6	37	19
Unsaturated	21	–	10	8	15	13
Total	65	15	40	14	52	32
T_m						
Saturated	72	37	72	36	68	47
Unsaturated	71	2	24	20	21	47
Total	143	39	96	56	89	94

2.2. Dataset

Experimental data on ΔH_f, T_m, on the crystal structure including SS and LS, and the GLY configuration of several TAGs were gathered from a public-domain literature review.[7,18,19,23–43] The review delivered a large number of T_m and ΔH_f data of saturated TAGs. Unfortunately, fewer data of unsaturated TAGs were identified. In total, experimental data for 282 TAGs were accumulated. This dataset was reduced by excluding TAGs containing odd chain lengths and chain lengths greater than 20. The resulting dataset *D* comprised 262 TAGs. These are 137 fully saturated TAGs and 125 TAGs containing at least one unsaturated fatty acid—referred to as "unsaturated" TAGs. **Table 2** summarizes the number of data available in literature that was used to generate dataset *D*.

No experimental data on ΔS_f, LS information on polyunsaturated TAGs, and SS information on TCL structures were

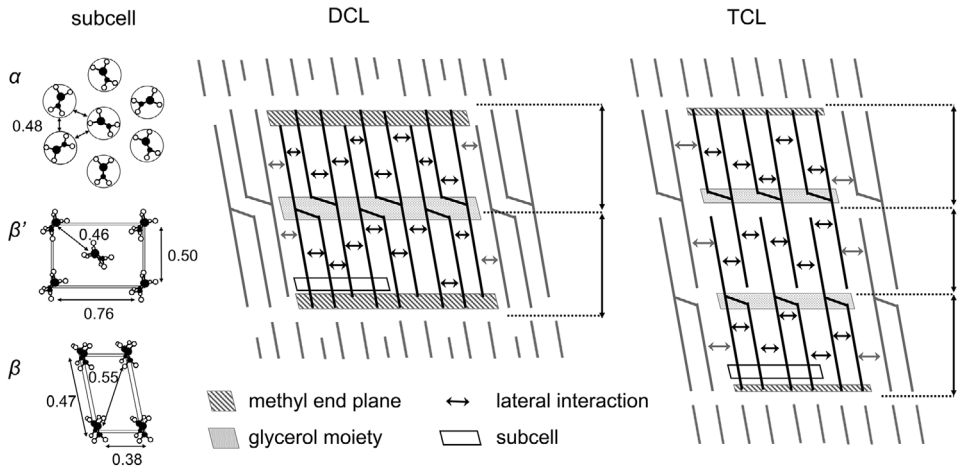

Figure 1. Subcells with geometrical dimensions and reference cells for DCL and TCL, unit nm.

available. ΔS_f data were generated by dividing the experimentally determined ΔH_f and T_m.

2.3. Model Setup

2.3.1. Enthalpy of Fusion

A linear dependence of ΔH_f on the total carbon number of saturated monoacid TAGs is generally acknowledged.[9,10] Since TAGs differ in saturation, GLY configuration, and chain length, the linear relation known for monoacid TAGs needs to be refined. ΔH_f is subdivided into three contributions: 1) the contribution of the INT between hydrocarbon chains (H_{INT}), 2) the contribution of the GLY (H_{GLY}), 3) the contribution of the MEP (H_{MEP}),

$$\Delta H_{\mathrm{f}} = H_{\mathrm{INT}} + H_{\mathrm{GLY}} + H_{\mathrm{MEP}} \quad (1)$$

In the following, the terms "hydrocarbon chain," "alkyl chain," "fatty acids" are used interchangeably.

On the basis of the linear relation valid for monoacid TAGs, a reference cell is defined. Reference cells were formulated for two basic crystal structures, DCL and TCL. Their sizes are defined by the characteristic carbon number *C* reflecting an "ideal" monoacid TAG (**Figure 1**). The characteristic carbon number is determined by the longest fatty acid in each leaflet. Obviously, in the TCL structure, two characteristic carbon numbers must be defined, one for the middle layer and one for the outer layer(s). In DCL, only one characteristic carbon number needs to be assigned as both layers mirror each other.

Consequently, the DCL and TCL structure is simplified by the "stacking" of two TAG molecules and subsequent molecules in the lateral direction. In this spirit, the reference cell does not reflect the true unit cell of the crystal which varies for every polymorph. From a review of single-crystal studies,[44] it can be deduced that no general unit cell of TAG crystals for each polymorph can be assigned. While for the β-polymorph triclinic unit cells containing two TAG molecules are generally reported, different unit cells (and subcells) composed of eight molecules for TAGs in the β'-polymorph are known. For example, CLC and PPM adapt an orthorhombic and monoclinic unit cell, respectively.[45,46] What is striking is the similarity of the two analyzed TAGs, both being saturated with small chain length differences, yet large structural differences in the crystalline state were found.

However, in the model presented in this contribution specific information on the unit cell is not included. ΔH_f is rather approximated using structural information on TAGs in the DCL and TCL structure as described above in three main polymorphic form — rendering six TAG-subcategories, that is, DCL in α, DCL in β', DCL in β-polymorph and analogously TCL. Based on CLM, symmetry, degree of saturation, and, primarily LS information, TAGs were assigned to named specific crystal structures using a decision tree based on the available experimental data.

INT: The contribution of the INT between hydrocarbon chain elements is assumed to be a function of their average lateral distance *d* in a crystal structure. No distinction is made between neighboring fatty acid moieties belonging either to the same or another TAG. Thus, the next neighbor fatty acids were identified by the subcell packing of the fatty acids in a crystal structure. The subcell information from XRD and wide-angle spectra is used for this purpose. The α-polymorph has a hexagonal subcell (H), which consists of freely rotating hydrocarbon chains. It reveals a single interplanar spacing of 0.415 nm. The β'-polymorph has an orthorhombic perpendicular subcell ($O_{\perp}$). The adjacent hydrocarbon chains are orientated orthogonally to each other. The XRD pattern shows two peaks that correspond to SS of 0.42 and 0.38 nm, respectively. The β-polymorph has a triclinic parallel subcell ($T_{//}$) with parallel aligned chain orientation. It yields peaks corresponding to SS around 0.46, 0.37, and 0.39 nm.[47]

The subcells can be simplified using basic geometry (α: hexagon, β': rectangular, β: parallelogram, see Figure 1). The arithmetic mean distance of the six next neighbors of the central chain was computed by a geometrical simplification (**Figure 2**).

Even though a hydrocarbon chain in the β' or β-polymorph has next neighbors in eight directions, the two most distant were disregarded because of their substantially larger distance to the central chain. This seems justified considering that the predominant van der Waals interaction decrease with the sixth power of the distance. The simplification led to an average lateral distance

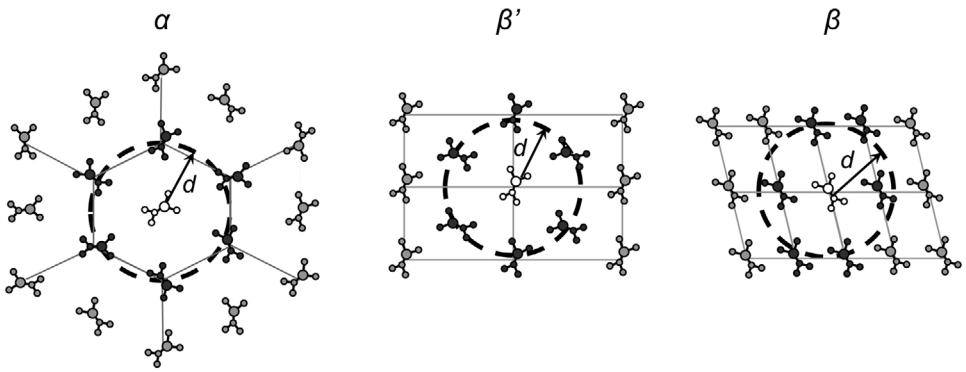

Figure 2. Geometrical simplification of subcell packing to estimate the average distance between adjacent fatty acids, predominantly interacting fatty acids (black), not interacting fatty acids (grey), interaction radius (dashed circle), average lateral distance (*d*).

of 4.79, 4.72, and 4.63 Å for the α-polymorph, β'-polymorph, and β-polymorph, respectively.

Further, the kind of hydrocarbon chain (i.e., degree of saturation) is considered in the description of the INT contribution. A combinatorial interaction parameter A is introduced to account for different combinations of saturated and unsaturated hydrocarbon chains. Only relevant for the DCL, the parameter A is computed as the weighted sum of the contributions A_{SS}, A_{SU}, and A_{UU}. These parameters represent the interaction between two saturated, one saturated and one unsaturated, and two unsaturated fatty acids, respectively.

The parameters A_{SU} and A_{UU} account primarily for oleic acid (single double bond in *cis*-configuration). For other typically occurring unsaturated fatty acids in TAGs, for example, elaidic acid (E), linoleic acid (l), and linolenic acid (le), correction factors, and switch-functions for the parameters A_{SU} and A_{UU} were introduced. This variation of the interaction parameter A is necessary to reflect the observation that the number of double bonds, their position, and the configuration (*cis* or *trans*) clearly affect T_m and ΔH_f of TAGs. The fact that ΔH_f of SES, SOS, and SlS in the α-polymorph is 96.2, 47.4, and 40.9 kJ mol^{-1}, respectively, illustrates this undoubtedly. Since these TAGs are symmetrical and most likely adapt the tuning fork configuration, differences in ΔH_f have to be accounted for by different INTs.

Different from the DCL, it is assumed that the TCL does not contain pairs of neighboring saturated and unsaturated fatty acids in the lateral plane. The TCL is rather characterized by different leaflets exclusively composed of either saturated or unsaturated fatty acids rendering the contribution A_{SU} in TCL obsolete. Thus, the middle layer and outer layers can be solely described by A_{SS} and A_{UU}.

GLY: The GLY adapts at least two major configurations, chair or tuning fork. These are also considered in the model. The contribution of the GLY to ΔH_f was incorporated by simply adding an extra term. This term represents by default the chair configuration and is varied via a switch-function and correction factor to account for the tuning fork configuration. A decision tree was used to assign a GLY configuration to a TAG. The decision tree follows this reasoning: 1) regarding saturated TAGs, the symmetry of the molecule determines the GLY configuration. Accordingly, an achiral or symmetric saturated TAG adapts the tuning fork configuration (e.g., PSP), while an asymmetric saturated TAG always adapts the chair configuration (e.g., MMP). 2) Unsaturated fatty acids do not form a mixed leaflet with saturated fatty acids in more stable polymorphs, that is, SOS adapts the tuning fork configuration, SOO the chair configuration. This is in line with literature reports.[43,48] In mixed-acid saturated TAGs, the GLY configuration is chosen in such a way that the relative CLM is minimized.

The GLY contributions in either DCL or TCL are distinguished but modeled in the same manner. It was assumed that the GLY contribution in these two crystal structures (DCL, TCL) is different in each polymorph. However, the main difference between the chair and tuning fork configuration of the GLY is considered of conformational and not of energetical nature. It was hence postulated that the relation of chair to tuning fork is constant throughout the different polymorphs and chain length configurations. This implies that seven parameters account for the contributions of the GLY to the enthalpy of fusion.

MEP: The length difference (i.e., difference in carbon numbers) in neighboring hydrocarbon chains is either zero for monoacid TAGs or non-zero for mixed-acid TAGs. The latter case causes disruptions in the MEP and creates voids that reduce the overall crystal energy.[16,49] This effect is accounted for in the description of the MEP in the model. Therefore, the CLM is introduced that describes the deviation of the actual hydrocarbon chains to the characteristic carbon number of the reference cell. This means that at least one CLM is zero.

In DCL, the CLM between each fatty acid and the longest fatty acid (characteristic carbon number of the reference cell) is considered. The CLM determined this way is thus assumed to be independent of the GLY configuration. In TCL, the CLM assessment is limited to the outer layer. Therefore, a pre-assignment of fatty acids to the different layers is required to allow the determination of the respective CLM next to the characteristic carbon number of each layer. A decision tree was developed to assign fatty acids to either the middle or outer layer(s).

The CLM was expressed as a relative CLM as a CLM of 2 has a greater effect on a TAG with a characteristic carbon number of 12 (e.g., CLL) than with 18 (e.g., PSS). Regarding models that build up properties additively from elements of chain molecules, one could be tempted to consider a void as an absolute length reduction of the interacting chains. For the model formulated here, it is emphasized that the void is accounted for as a correction for the

"perfectly" filled reference cell and, hence, results in relative perturbation. After careful geometrical assessment, the angle of tilt, τ, of the hydrocarbon chains with respect to the lamellar interface was incorporated into the model as well. This tilt can be interpreted as scaling factor of the potential voids due to increasing chain inclination (decreasing angle) with increasing stability of the polymorph, expressed as $\sin(\tau)$. According to literature data of the α, β', and β-polymorph, the angles were approximated by 90°, 70°, and 60°, respectively.[44,50] The MEP contribution has an upper bound asymptotically approached with increasing relative CLM.

2.3.2. Melting Temperature

To formulate a model to predict or rather correlate T_m of pure TAGs, two approaches have been reported. In the first approach, the experimental available T_m are used to derive a parameter set for a physically meaningless equation that reproduces the data. The second approach is based on the thermodynamically consistent relation of the three quantities ΔH_f, ΔS_f, and T_m at phase equilibrium,

$$\Delta G = 0 = \Delta H_\mathrm{f} - T_\mathrm{m}\,\Delta S_\mathrm{f} \tag{2}$$

$$T_\mathrm{m} = \frac{\Delta H_\mathrm{f}}{\Delta S_\mathrm{f}} \tag{3}$$

To follow this route of modeling, expressions to describe ΔS_f need to be formulated. Typically, this is done analogously to the models for ΔH_f. This route includes deriving ΔS_f data following Equation (2) from ΔH_f and T_m and subsequent parameter optimization. Even though questionable, it is certainly more intuitive to model ΔS_f by a group contribution approach. Anyhow, both approaches involve the determination of several additional parameters seeking a consistent description and prediction of T_m.

In this work, another approach is followed. From *n*-alkanes and other related homologous alkyl-series, a linear correlation of ΔH_f and ΔS_f was retrieved. This relation is obvious if both properties scale linearly with the number of carbons in the alkyl chain. This is also valid for saturated monoacid TAGs.[51] Thorough analysis of the available experimental data (ΔH_f and T_m), from which ΔS_f data were generated, revealed that this linear correlation strikingly also holds for other types of TAGs, mixed-acid, and also the data of unsaturated TAGs, see **Figure 3**. The fact that also the data relating to different polymorphic forms of the same TAGs can be described by one common linear fit is even more surprising. For more details, readers are referred to another manuscript of ours.[52]

In the model presented in this contribution, the relation between the ΔH_f and ΔS_f is straightforwardly captured in a linear relation,

$$\Delta S_\mathrm{f} = x\,\Delta H_\mathrm{f} + y \tag{4}$$

Finally, T_m for any TAG is derived based on the values obtained for ΔH_f in combination with Equation (4) substituted into Equation (3). Although the data for saturated and unsaturated TAGs are overall well represented by a single fit for Equation (4), there

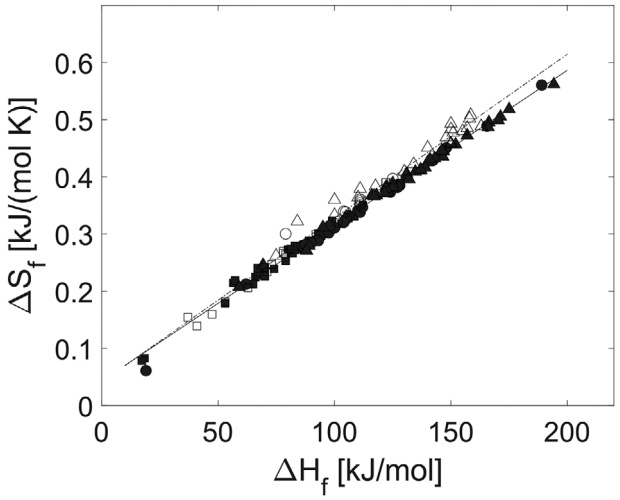

Figure 3. ΔS_f versus ΔH_f for saturated (filled) and unsaturated TAGs (empty), α-polymorph (squares), β'-polymorph (circles), β-polymorph (triangles), representation of the linear relation of ΔS_f versus ΔH_f indicated for saturated TAGs (solid line) and unsaturated TAGs (dashed line).

appears to be a systematic difference between these sets of experimental data (see Figure 3). Consequently, the parameters x and y of Equation (4) for saturated and unsaturated TAGs were determined as part of the optimization procedure. Even though Equation (4) certainly deserves a more detailed discussion, it is taken as an observational fact here. For an adequate discussion, the reader is referred to another manuscript of ours[52] as this is considered beyond the scope of this contribution.

2.4. Model Structure

The model input is the TAG including the information on the constituting fatty acids and their position on the GLY. This information is used to pre-assign a crystal structure and a GLY configuration using generalized decision trees. Based on this, internal function variables as the characteristic carbon number C and CLM are defined. Subsequently, the enthalpy of fusion is computed as follows,

$$\mathrm{DCL}:\ \Delta H_\mathrm{f}^{\{k\}} = \frac{A}{d^{\{k\}6}}\,C + g^{\{k\}}\,\left(1 + g_\mathrm{tf}\,f_\mathrm{tf}\right) + c^{\{k\}}\,\sum_{i=1}^{3}\tanh\left(\left(\sin\tau^{\{k\}}\,\frac{CLM_i}{C}\right)^{a^{\{k\}}}\right) \tag{5}$$

$$\mathrm{TCL}:\ \Delta H_{f,tr}^{\{k\}} = \frac{1}{3}\,\frac{A_\mathrm{middle}}{d^{\{k\}6}}C_\mathrm{middle} + \frac{2}{3}\,\frac{A_\mathrm{outer}}{d^{\{k\}6}}C_\mathrm{outer} + g_{tr}^{\{k\}}\,\left(1 + g_{tf}\,f_{tf}\right) + c_{tr}^{\{k\}}\,\tanh\left(\left(\sin\tau^{\{k\}}\,\frac{CLM_{tr}}{C_{outer}}\right)^{a_{tr}^{\{k\}}}\right) \tag{6}$$

Where the superscript k denotes the respective polymorph $\{k = \alpha, \beta', \beta\}$, the subscript tr describes ΔH_f computed for TAGs

Table 3. Expression for the interaction parameter A in DCL for different TAG subcategories.

Subcategory	Expression
SSS	$A = A_{SS}$
SSU/SUS/USS	$A = \frac{4}{9} A_{SS} + \frac{4}{9} A_{SU} (1 + p_E f_E + p_l f_l + p_{le} f_{le}) + \frac{1}{9} A_{UU}(1 + p_E f_E + p_l f_l + p_{le} f_{le})$
SUU/UUS/USU	$A = \frac{1}{9} A_{SS} + \frac{4}{9} A_{SU} (1 + p_E f_E + p_l f_l + p_{le} f_{le}) + \frac{4}{9} A_{UU}(1 + p_E f_E + p_l f_l + p_{le} f_{le})$
UUU	$A = A_{UU}$

S denotes a saturated fatty acid, U denotes an unsaturated fatty acid; A_{SS} (interaction between two saturated fatty acids), A_{SU} (interaction between one saturated and one unsaturated fatty acid), A_{UU} (interaction between two unsaturated fatty acids); subscripts: E (eladic acid), l (linoleic aicd), le (linolenic acid).

in the TCL structure, C is the characteristic carbon number in each leaflet, A is the interaction parameter, τ is the angle of tilt with generalized values of 90°, 70°, and 60° for the α-, β'-, and β-polymorph, respectively, and d describes the average lateral distance of 4.79, 4.72, and 4.63 Å for the α-polymorph, β'-polymorph, and β-polymorph, respectively. The parameter g accounts for the GLY contribution, c and a account for the MEP contribution. The $\sin(\tau)$ was introduced as a geometrical scaling factor of the occurring voids in mixed-acid TAGs. The hyperbolic tangent function was chosen as the MEP contribution is believed to increase asymptotically on increasing CLM. In the equation to calculate the enthalpy of fusion in the TCL structure, the weights 1/3 and 2/3 were included because the TCL is composed of one middle layer and two outer layers.

In DCL, the interaction parameter A is approximated by

$$A = w_1 A_{SS} + w_2 A_{SU} \left(1 + p_E f_E + p_l f_l + p_{le} f_{le}\right) + \left(1 - w_1 - w_2\right) A_{UU} \left(1 + p_E f_E + p_l f_l + p_{le} f_{le}\right) \quad (7)$$

where w_1 and w_2 are weights determined by combinatorics. The parameters p_E, p_l, and p_{le} account for elaidic (subscript E), linoleic (subscript l), and linolenic (subscript le) acid and the respective switch-functions f_E, f_l, and f_{le} are 1 if elaidic, linoleic and linolenic acid is present, respectively. The detailed expressions for the different subcategories can be found in **Table 3**.

In TCL, the interaction parameters A_{middle} and A_{outer} are either determined by the contribution A_{SS} or A_{UU} exclusively, as derived in Section 2.3. Again, the parameter A_{UU} is altered depending on the type of unsaturated fatty acid present,

$$A_{middle} = A_{UU,middle} \left(1 + p_{E,middle} f_{E,middle} + p_{l,middle} f_{l,middle} + p_{le,middle} f_{le,middle}\right) \quad (8)$$

$$A_{outer} = A_{UU,outer} \left(1 + p_{E,outer} f_{E,outer} + p_{l,outer} f_{l,outer} + p_{le,outer} f_{le,outer}\right) \quad (9)$$

T_m is computed as described in Section 2.3.2 according to Equations (3) and (4) as a function of ΔH_f,

$$T_m = \frac{\Delta H_f}{x \Delta H_f + \gamma} \quad (10)$$

It has to be noted that this relation is independent of the crystal structure, that is, DCL or TCL, and polymorphic form. For the calculations discussed in this manuscript, independent parameters for saturated and unsaturated TAGs were employed though. The other variables only affect the values computed for ΔH_f.

In summary, the model formulated requires 39 parameters. Based on this parameter set, the output for any TAG is a vector containing ΔH_f and T_m for the three polymorphic forms.

2.5. Model Fit Procedure

The model parameters were fit to experimental ΔH_f and T_m data (dataset D). The model equations for ΔH_f and T_m are coupled. To optimize the determination of the model parameters, all available experimental data were used in the fit procedure. It has to be pointed out here that the whole parameter set of the model is determined by a single optimization run. This is intrinsic to the model because several single parameters cover practically all experimental data points, see Supporting information for details on the derived parameters. The often-used output least-squares approach was employed with equally weighted data. The model parameters were fit to the experimental dataset using once an unconstrained (I), once a constrained (II) optimization scheme. The latter enforces thermodynamic constraints on the model output to ensure thermodynamic consistent model predictions. The criteria for consistency are formulated in Equations (11) and (12) and related to the relative stability of the polymorphs,

$$\Delta H^{\alpha}_{f,TAG} < \Delta H^{\beta'}_{f,TAG} < \Delta H^{\beta}_{f,TAG} \quad (11)$$

$$T^{\alpha}_{m,TAG} < T^{\beta'}_{m,TAG} < T^{\beta}_{m,TAG} \quad (12)$$

The necessity of performing a constrained model fit was first proposed by Moorthy et al.[22] From each model fit, a parameter set was derived, denoted as P^{I} (unconstrained) and P^{II} (constrained), respectively. For more details concerning the mathematical point of view, see Supporting information.

2.6. Numerical Assessment of Model Performance

The model performance was assessed in terms of the prediction quality, thermodynamic consistency of the model predictions, and the predictive power of the model. The prediction quality was determined for subcategories of TAGs: 1) saturated TAGs in α-polymorph, 2) saturated TAGs in β'-polymorph, 3) saturated TAGs in β-polymorph, and analogously for unsaturated TAGs. This resulted in six subcategories of respective sample size N_{cat}. The root-mean-square error (RMSE) was computed from experimental and predicted data,

$$RMSE = \sqrt{\frac{\sum (l_{EXP} - l_{PRED})^2}{N_{cat}}} \quad (13)$$

where l is either T_m or ΔH_f and N_{cat} is the size of the respective category. Further, the ratio of overpredictions O to

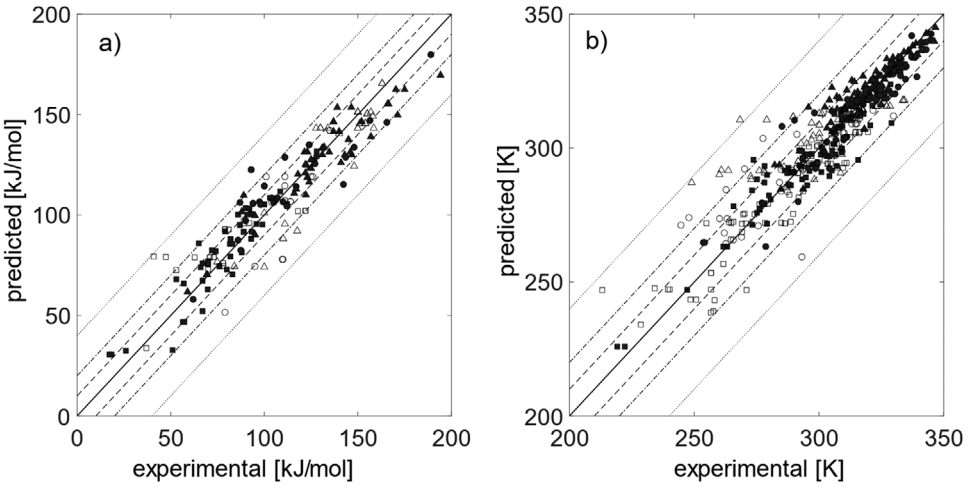

Figure 4. Predictions for a) ΔH_f in kJ mol^{-1} and b) T_m in K of saturated TAGs (filled) and unsaturated TAGs (empty) in α-polymorph (squares), β'-polymorph (circles), and β-polymorph (triangles) estimated by the model proposed in this work (parameter set P^{II}). The solid black line indicates the perfect prediction, with dashed, dash-dotted, and dotted lines representing deviations of ±10 units, ±20 units, and ±40 units, respectively.

underpredictions U was considered,

$$\frac{O}{U} = \frac{\text{number of over predictions}}{\text{number of under predictions}} \tag{14}$$

Over predictions are those greater than the respective experimental data point, conversely, under predictions are smaller than the experimental data point.

Additionally, the residual (δ) was tabulated:

$$\delta = l_{\text{EXP}} - l_{\text{PRED}} \tag{15}$$

The thermodynamic consistency of the predicted properties, Equations (11) and (12), was expressed by a "score", denoted as TC. If the predictions for a single TAG in all three possible modifications (α, β', β) were found to be consistent, the TAG was assigned a score of 1. Conversely, if at least one inconsistency is identified the TAG is assigned a score of 0. The overall score of TC was introduced,

$$TC = \frac{\text{number of TAGs assigned score 1}}{\text{total number of TAGs in category}} \tag{16}$$

Different from assessing the prediction quality, which depends on the availability of the experimental data, the TC score could be determined for all TAGs in the dataset.

The predictive power of the model was examined by fitting the model to a smaller dataset D' (randomly chosen TAGs) and comparing the measures of the prediction quality to the model parameters when the model fit was performed on the broad dataset D. The dataset D' comprised 188 TAGs covering about equal numbers of saturated (92) and unsaturated (96) TAGs.

3. Model Performance

3.1. Predictions Quality and Thermodynamic Consistency

The model performance was assessed by evaluating measures of prediction quality (RMSE, U/O, O/U) and the TC score of ΔH_f and T_m predictions. The prediction quality measures were compared to the model proposed by Wesdorp[6] and revised by Moorthy et al.[22] as reference model. To calculate the thermodynamic properties using this reference model, the parameter set given in[22] and ΔS_f model to compute T_m was used. For detailed information on this model, the reader is referred to the aforementioned references.

The prediction quality of the model proposed in this contribution is illustrated in **Figure 4**. The parity plots for ΔH_f (a) and T_m (b) consider predictions obtained by the constrained model fit (P^{II}). The display of the predictions resulting from P^{II} was in particular chosen to highlight the differences between the predictions of saturated and unsaturated TAGs. Similar parity plots were obtained using P^{I}.

The RMSE and the ratio of overprediction to underprediction (O/U, U/O) of the two parameter sets of the new model (I: unconstrained, II: constrained) and the reference model are tabulated in **Table 4**. The ideal value of RMSE indicating a perfect prediction would be zero and for both ratios 1. Regarding the latter, other values indicate systematic deviations.

As Table 4 reveals, the unconstrained and constrained model fit resulted in model predictions of comparable quality. For saturated TAGs, the RMSEs of ΔH_f predictions vary between 8 and 13 kJ mol^{-1} for all polymorphs. For unsaturated TAGs, the RMSE is greater than for saturated TAGs, varying from 12 to 16 kJ mol^{-1}. The RMSEs for T_m predictions vary from 5 to 7 K and 9 to 14 K for saturated and unsaturated TAGs, respectively. Overall, the small RMSE indicates a good reproduction of the experimental data of both quantities by the new model.

The ratio of overpredictions to underpredictions was found to be the largest for the T_m of unsaturated TAGs in the α-polymorph—O/U of 1.92 (I) and 2.17 (II)—indicating a systematic overestimation. The T_m of saturated TAGs in the β-polymorph were found to be underestimated with an O/U of 0.49 (I) and 0.42 (II). Also, the ΔH_f predictions for saturated TAGs in the α-polymorph was found to be systematically too small, O/U 0.44 (I) and 0.40 (II).

European Journal of Lipid Science and Technology
www.ejlst.com

Table 4. Summary of prediction quality measures for enthalpy of fusion (ΔH_f: RMSE in kJ mol^{-1}) and melting temperature (T_m: RMSE in K) predictions approximated by the new model using P^{I} (I: unconstrained) and P^{II} (II: constrained), and by the reference model, predictions were obtained for dataset *D*.

			Saturated			Unsaturated		
			α	β'	β	α	β'	β
Reference								
	ΔH_f	RMSE	7.65	9.77	9.81	18.66	13.74	11.12
		O/U (U/O)	1.27 (0.79)	0.57 (1.77)	0.60 (1.67)	0.75 (1.33)	0.50 (2.00)	0.27 (3.67)
	T_m	RMSE	7.54	4.81	2.60	13.11	9.86	6.07
		O/U (U/O)	0.38 (2.63)	0.27 (3.70)	1.25 (0.80)	1.03 (0.97)	0.38 (2.67)	1.06 (0.94)
New model								
P^{I}	ΔH_f	RMSE	8.86	12.68	9.45	15.92	14.90	12.02
		O/U (U/O)	0.44 (2.28)	0.64 (1.57)	1.15 (0.87)	0.62 (1.63)	1.25 (0.80)	1.33 (0.75)
	T_m	RMSE	6.57	5.90	5.67	9.85	11.56	13.40
		O/U (U/O)	1.22 (0.82)	1.51 (0.66)	0.49 (2.03)	1.92 (0.52)	1.75 (0.57)	0.89 (1.13)
P^{II}	ΔH_f	RMSE	8.91	12.61	11.26	15.84	15.51	11.58
		O/U (U/O)	0.40 (2.47)	0.80 (1.25)	1.43 (0.70)	0.62 (1.63)	1.25 (0.80)	1.33 (0.75)
	T_m	RMSE	6.74	5.82	5.39	10.15	11.82	13.60
		O/U (U/O)	1.18 (0.85)	1.84 (0.54)	0.42 (2.38)	2.17 (0.46)	1.59 (0.63)	0.74 (1.34)

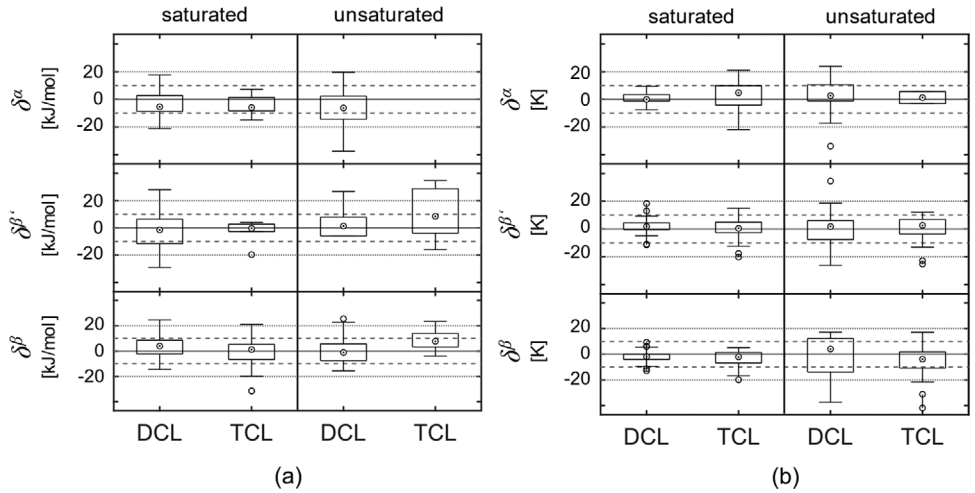

Figure 5. Comparison of the residuals δ of a) ΔH_f predictions in kJ mol^{-1} and b) T_m predictions in K obtained using P^{II} for saturated and unsaturated TAGs approximated in DCL and TCL. Dashed and dotted lines in grey are added to guide the eye. Boxplots show the median, 0.25 and 0.75 quartiles as bottom and top edges, vertical lines give the extend of the errors for values that are no outliers, outliers shown as circles. No experimental ΔH_f data were available for unsaturated TAGs adapting the TCL structure in the α-polymorph.

Table 3 also displays the values obtained for the reference model. At first instance, the values obtained for both models are similar. This holds in particular for ΔH_f. However, for the T_m of saturated and unsaturated TAGs, both in the β-polymorph, the reference model outperforms the new model—RMSE of 2.6 K compared to 5.7/5.4 K (I/II) and 6.1 K to 13.4/13.6 K (I/II). However, considering the score of over- to under predictions (O/U), the reference model performs actually less good than the new model. Values smaller than 0.5 and greater than 2.0 are considered to indicate a systematic error of prediction. For the reference model, four out of 12 O/U values covering different TAG-subcategories reveal a strong bias of the predictions. For the proposed model, two (I) and three (II) out of 12 O/U values indicate a systematic error. Regarding this comparison, the fact that the number of adjustable parameters in the reference model is twice that of the proposed model—39 versus 84—cannot be ignored.

Figure 5 shows a comparison of the residuals of computed ΔH_f and T_m to experimental data for saturated and unsaturated TAGs. The residuals are depicted as boxplots comprising the median, 0.25 and 0.75 quartiles, the extent of errors that are no outliers, and outliers. The DCL and TCL were assigned according to a decision tree. The estimates were obtained using P^{II}, similar results were obtained for P^{I}.

From Figure 5 can be derived that good predictions for the ΔH_f of saturated TAGs in DCL and TCL were obtained. For unsaturated TAGs, the prediction of the ΔH_f in DCL was found to be

Table 5. Summary of prediction quality measures for enthalpy of fusion (ΔH_f: RMSE in kJ mol^{-1}) and melting temperature (T_m: RMSE in K) estimates obtained using P^{I} (I: unconstrained) and P^{II} (II: constrained). The model fit was performed on dataset D' and the predictions obtained for the broad dataset D.

			Saturated			Unsaturated		
			α	β'	β	α	β'	β
I	ΔH_f	RMSE	8.59	12.22	9.74	16.24	15.25	11.56
		O/U (U/O)	0.44 (2.28)	0.80 (1.25)	1.07 (0.93)	0.62 (1.63)	1.25 (0.80)	1.33 (0.75)
	T_m	RMSE	6.47	5.95	5.93	10.10	12.19	13.47
		O/U (U/O)	1.10 (0.91)	1.00 (1.00)	0.39 (2.59)	2.32 (0.43)	1.59 (0.63)	0.94 (1.06)
II	ΔH_f	RMSE	8.59	12.36	10.82	15.96	16.04	11.03
		O/U (U/O)	0.44 (2.28)	0.89 (1.12)	1.43 (0.70)	0.62 (1.63)	1.25 (0.80)	1.33 (0.75)
	T_m	RMSE	6.57	5.86	5.90	10.55	12.59	13.71
		O/U (U/O)	1.22 (0.82)	1.40 (0.71)	0.42 (2.38)	3.29 (0.30)	1.59 (0.63)	0.79 (1.27)

quite good as well. The prediction for the TCL structure appears to be of much lesser quality. The deviations found for the T_m predictions of unsaturated TAGs are larger than those for saturated TAGs. Contrarily to the saturated TAGs, data on the TCL structure of unsaturated TAGs are better reproduced by the model than those for the DCL packing. This is most apparent for the β-polymorph. Generally, the unsaturated TAGs which are mostly considered comprise a mixture of fatty acids covering saturated and unsaturated. These are most often distributed over different leaflets rendering the TCL structure in more stable polymorphic forms. Unsaturated TAGs which adapt the DCL structure in the β-polymorph are typically composed of exclusively unsaturated fatty acids, for example, OOO. These are extreme cases characterized by low T_m and consequently of limited importance.

For the model fit without enforcing thermodynamic constraints (parameter set P^{I}), thermodynamic consistency was not given for all predictions. For saturated and unsaturated TAGs, a TC score of 0.934 and 0.856 was obtained, respectively. Enforcing thermodynamic consistent model predictions (parameter set P^{II}) intrinsically resulted in a score of 1. Considering Table 3, it appears that the enforced satisfaction of these constraints does not alter the prediction quality much. Data for the ΔH_f generated with the reference model were consistent for saturated TAGs and unsaturated TAGs—TC score of 1. The reference model, however, yields much less consistent data for T_m resulting in a TC score of 0.745 and 0.376 for saturated and unsaturated TAGs, respectively. It is known that this model was not developed taking these constraints into account.

3.2. Predictive Power

The predictive power of the model was examined by fitting the model to a reduced dataset D' which contains randomly chosen TAGs from dataset D. The obtained parameter set was used to calculate the thermodynamic properties for TAGs in the broad dataset D. The prediction quality measures are summarized in **Table 5**.

Although only 188 TAGs (dataset D') were used for parameter optimization, differences between the resulting model performance on the complete dataset are small, comparing Tables 3 and 5. The largest changes were found when predicting T_m of unsaturated TAGs in the α-polymorph. For both, the unconstrained and the constrained fit, a drift toward overestimation is indicated by O/U values of 2.32 and 3.29, respectively. Overall, this test, though far from conclusive, indicates robustness of the parameter set and, thus, good extrapolation capability/predictive power of the model.

4. Discussion

4.1. Model Parameters

The parameters obtained are given in Table S1, Supporting information. It must be noted that not all parameters actually present in the model formulated based on configurational assessment are addressed in the setup presented here. These remain idle due to lack of experimental data. This holds for example for TAGs in TCL packing containing elaidic acid in the β'-polymorph. In the following, some specific parameters obtained from the model fit constrained for thermodynamical consistency (P^{II}) are discussed. P^{II} is due to the thermodynamically consistent predictions considered superior to P^{I}. Hence, the latter becomes of lesser importance in this contribution. Before discussing the obtained parameter values, it should be stressed that constrained optimization implies here that only the model output was constrained, while no restrictions on the values of parameters were imposed. Next to the thermodynamic consistency, which is intrinsic to the model fit, it is interesting to evaluate if the evolution of values for specific parameters originating from the fit is in line with expectations.

First considerations deal with the general interaction parameter, A, describing the INT of a pair of carbon atoms located in adjacent chains. In the DCL, one could expect that this is highest for neighboring saturated chains. The unbiased optimization yields A_{SS} larger than A_{SU} and A_{UU}. This is thus in line with expectations. To formulate an expectation concerning the relative contributions A_{SU} and A_{UU} is practically impossible. In TCL, the model fit yielded larger values for the parameters of the middle layer ($A_{SS,middle}$, $A_{UU,middle}$) compared to the parameters of the outer layer. This can be explained by higher conformational freedom of the separated fatty acids in the middle layer. Opposed to this, the remaining fatty acids in the outer layer are

restricted due to their configuration being "locked" by the GLY configuration.

Regarding the interaction of two neighboring oleic acids, it is fair to expect a higher value in the TCL than in the DCL packing, since the first represents a middle layer exclusively composed of oleic acid. With values of 0.045 and 0.064 for A_{UU} and $A_{UU,middle}$ this expectation is met. Looking into more detail of the contributions of unsaturated fatty acids, the optimized parameters meet expectations well. The values of the parameters p_E, p_l, p_{le} indicate that elaidic has a larger contribution than oleic acid but that linoleic and linolenic contribute subsequently less than oleic acid. This, however, only holds for the DCL. With the average lateral distance derived from crystal structural information, the model also yields that the INT contribution is increasing with polymorph stability as expected.

Contrary to the general INT contribution, which is independent of the polymorph but modified by the characteristic average distance d, the parameters accounting for the GLY contribution were adjusted for each polymorph. The GLY is the only element of TAGs with a permanent dipole moment. This results in long-range induction forces stabilizing the molecule in both liquid and solid-states additional to the van der Waals-forces. In a study by Pink et al.,[53] it was suggested that in the liquid state clusters for non-zero attractive glycerol-glycerol forces are formed. This suggests that glycerol-glycerol interactions are more favored in the liquid state rather than in the confined solid-state. Building on this and approaching this problem somehow innocently, it seems fair to assume negative values for the GLY contribution to ΔH_f. In doing so it would be consequent to expect that the absolute value develops according to the increasing density of the TAG crystals with increasing polymorph stability, $g^{\alpha} < g^{\beta'} < g^{\beta}$. The parameter values derived for the TCL structure, $g^{\alpha} = -157$ kJ mol^{-1}, $g^{\beta'} = -437$ kJ mol^{-1}, $g^{\beta} = -925$ kJ mol^{-1} match this expectation. However, for the DCL structure, the picture emerging is less convincing. All three contributions are negative, but the absolute values are not systematic, 34, 876, and 9, respectively. Considering the massive simplification of the crystal structures inherent to the model presented and the variability and complexity, this mismatch in DCL is less surprising than the values obtained for TCL.

Taking the setup of the model into account, the contribution based on the CLM has to be negative as it corrects the ΔH_f value with respect to one of an ideal monoacid TAG. One would also expect the assigned absolute value to increase with increasing stability of the polymorph. The parameters derived from the optimization clearly do not obey these rules. For the DCL, the values for the α- and β-polymorph meet the expectations but for β' the value is positive and greater than for the β-polymorph. For the TCL packing, the sequence of the absolute values $c^{\alpha} < c^{\beta'} < c^{\beta}$ is in line with expectation. The fact that all three values are positive indicates, a certainly wrong, increasing effect of crystal packing imperfections to ΔH_f.

4.2. Model Evaluation

The model presented in this study was compared to a reference model which can be considered as the current standard.[5,22] Both models allow predicting the thermodynamic properties, namely ΔH_f and T_m, of pure TAGs in a comprehensive manner. This implies that the parameter sets derived from optimization to the available experimental data allow computing the properties for any TAG in the polymorphic forms α, β', and β. Despite some similarities, the new model is conceptionally quite different from the reference. In essence, the reference model is a composition of independent models per polymorph with disconnected parameter sets. In contrast, the model presented in this work uses for example a single set of optimized parameters for the mutual interaction of chain elements. The contributions of the interaction parameters, A_{SS}, A_{SU}, and A_{UU}, are specifically modulated per polymorph based on available geometrical data characteristic for each polymorph.

In line with other modeling attempts for ΔH_f, both models compute these by summation of different contributions. The new model, however, more clearly assigns these to specific molecular elements. This allows relating the parameters resulting from optimization to theoretical considerations concerning this contribution. For example, the contribution of the GLY to ΔH_f is expected to be negative what the optimization without any bias has yielded as well. Another difference between the two models is the chosen structural standard. The reference model emphasizes the lateral chain contribution by choosing polyethylene as a "standard state." In this contribution, the reference cell is essentially defined by an ideal monoacid TAG based on the longest chain present. These differences in the approach also propagate into the way the differences in chain lengths are accounted for. Further, the proposed model distinguishes between the DCL and TCL packing of TAGs.

In the new model, T_m is determined as a function of the computed ΔH_f. To do so, a newly formulated simple relation between ΔH_f and ΔS_f is employed.[52] In contrast, the reference model computes T_m as the ratio of ΔH_f and ΔS_f. To enable this, another set of independent model equations and parameters to calculate ΔS_f for different polymorphs are necessary. Even though both models allow to calculate properties for any TAG, the new model is considered less arbitrary because it is not based on several independent model equations/submodules. Consequently, it is anticipated that the new model will be able to predict the relative stability of the different configurations a TAG can assume properly.

The new model contains 39 adjustable parameters to predict six properties, the pair of T_m and ΔH_f for any TAG in three polymorphs. Even though ΔS_f are generated as well, these are not considered a relevant output. To deliver essentially the same information, the reference model uses 84 parameters. Admittedly, the description of the experimental data using the new model is not better than for the reference model. Considering the large dataset for which predictions are obtained (being 262 TAGs) and the drastic difference in the number of adjustable parameters (84 versus 39), it seems not justified to compare simply the RMSE for each subcategory. A true comparison can be made of both models taking into account the overall prediction error and the number of parameters. In this spirit, a corrected RMSE is computed,

$$RMSE_{corr} = \sqrt{\frac{\sum (l_{EXP} - l_{PRED})^2}{N - M}} \tag{17}$$

where l is either T_m or ΔH_f, N is the number of data points, and M the number of parameters. The reference model yields an $RMSE_{corr}$ of 14.05 kJ mol^{-1} and 8.16 K for the ΔH_f and T_m predictions. The corrected $RMSE_{corr}$ of the predictions for the new model is with 13.12 kJ mol^{-1} and 8.93 K a bit better. Even though the set of experimental data used in this effort has been composed carefully, the interpretation of the performance of the models has to consider the quality of the experimental data.

The model predictions obtained with the parameter set of the constrained fit (P^{II}) yield an optimal TC score of 1 as an intrinsic consequence. This is also true for ΔH_f predictions of the reference model. However, in terms of consistency of the T_m predictions, the new model clearly outperforms the reference model which yields values of 0.745 and 0.376 for saturated and unsaturated TAGs, respectively. In summary, the new model utilizes less than half the number of adjustable parameters, reproduces the experimental data in a comparable way, and is in itself thermodynamically more robust and consistent than the reference model. It appears hence fair to conclude that the new model outperforms the reference model.

5. Conclusion

In conclusion, this work demonstrates that different contributions to the thermodynamic properties can be expressed by means of repetitive structural attributes of pure TAGs deduced from molecular structures. It could also be shown that the obtained parameter values in most cases fall into expected ranges defined by carefully formulated assumptions. The number of adjustable parameters was successfully minimized to less than half compared to the well-known model by Wesdorp.[6] Correcting the RMSE to enable a true comparison of both models revealed that the new model surpasses the reference model in terms of prediction quality and thermodynamic consistency of the predictions.

Clearly, further refinement necessitates additional research to determine molecular structures that are not accessible to date, for example, XRD-analyses of TAGs adapting the TCL stacking. It is especially of interest, whether the middle and outer layers show different SS. Also, generally more data on LS of poly-unsaturated TAGs would support a more cohesive assignment of DCL or TCL configurations. An extension of the proposed model to other polymorphic forms, for example, sub-α, γ, is possible if the respective crystal characteristics are known and experimental data are available.

Finally, some potential limitations need to be considered. Obviously, some configurational and geometrical simplifications were made (see Section 2.3.1). Despite this fact, it could be shown that a lot of parameters can be related to a physical meaning. This could allow either to derive parameters differently than described here or to verify them independently. It has to be pointed out here that for the type of models like the one presented the quality of available experimental data is of utmost importance. Even though the data set has been carefully composed of literature data, its limitation strongly influences the determination of the adjustable parameters and the evaluation of the model quality.

The data derived using the new model are of value by themselves. However, the benefit of consistent and reliable predictions of pure component properties is elsewhere. Such a database is a prerequisite for any meaningful effort to predict the SFC in TAG mixtures. Likewise, it is also important to assess the driving forces in crystallization processes such as rate of nucleation and growth. The approach of defining a reference cell developed in the proposed model can be expanded to binary mixtures and, thus, be used to find expressions for the non-idealities in solid TAG phases.

Abbreviations

CAT, category; CLM, chain length mismatch; DCL, double chain length crystal structure; DSC, differential scanning calorimetry; EXP, experimental; GLY, glycerol backbone; INT, lateral interaction; LS, long spacing; MEP, methyl end plane; PRED, prediction; SS, short spacing; SFC, solid fat content; T_m, melting temperature; TAG, triglyceride; TCL, triple chain length crystal structure; XRD, X-ray diffraction; ΔH_f, enthalpy of fusion; ΔS_f, entropy of fusion

Supporting Information

Supporting Information is available from the Wiley Online Library or from the author.

Acknowledgements

The authors thank Dr. Anthony J. Kearsley (Applied and Computational Mathematics Division, National Institute of Standards and Technology) and Dr. Arun S. Moorthy (Biomolecular Measurements Division, National Institute of Standards and Technology) for their assistance with parameter optimization and overall guidance regarding the mathematical point of view.

Conflict of Interest

The authors declare no conflict of interest.

Author Contributions

J.S.: conceptualization, data curation, formal analysis, investigation, methodology, project administration, resources, software, supervision, validation, visualization, writing-original draft, writing-review & editing.

Data Availability Statement

The data that support the findings of this study are available from the corresponding author upon reasonable request.

Keywords

crystal structure, enthalpy of fusion, group contribution, mathematical modeling, melting temperature, triglyceride properties

Received: January 19, 2021
Revised: May 29, 2021
Published online: June 24, 2021

[1] E. Flöter, *Eur. J. Lipid Sci. Technol.* **2009**, *111*, 219.
[2] M. Teles dos Santos, P. Morgavi, G. A. Le Roux, *OCL: Oilseeds Fats, Crops Lipids* **2018**, *25*, D107.

[3] M. Teles dos Santos, V. Gerbaud, G. Le Roux, *Chem. Eng. Sci.* **2013**, *87*, 14.
[4] P. E. Augusto, B. M. Soares, M. C. Chiu, L. A. Gonçalves, *Food Res. Int.* **2012**, *45*, 132.
[5] J. L. Hjorth, R. L. Miller, J. M. Woodley, S. Kiil, *J. Am. Oil Chem. Soc.* **2015**, *92*, 17.
[6] L. H. Wesdorp, Doctoral Thesis, Delft University of Technology, **1990**.
[7] C. K. Zéberg-Mikkelsen, E. H. Stenby, *Fluid Phase Equilib.* **1999**, *162*, 7.
[8] J. W. Hagemann, J. A. Rothfus, *J. Am. Oil Chem. Soc.* **1983**, *60*, 1123.
[9] M. Ollivon, R. Perron, *Thermochim. Acta* **1982**, *53*, 183.
[10] R. E. Timms, *Chem. Phys. Lipids* **1978**, *21*, 113.
[11] S. M. Mirpoorian, M. Vakili, S. H. Noie Baghban, P. Roohi, *J. Therm. Anal. Calorim.* **2019**, *137*, 679.
[12] E. Pereira, F. T. Junqueira, A. J. d. A. Meirelles, G. J. Maximo, *Fluid Phase Equilib.* **2019**, *493*, 58.
[13] M. Teles dos Santos, G. A. C. Le Roux, V. Gerbaud, *J. Am. Oil Chem. Soc.* **2011**, *88*, 223.
[14] K. Larsson, *Fette, Seifen, Anstrichm.* **1972**, *74*, 136.
[15] M. Sasaki, S. Ueno, K. Sato, in *Cocoa Butter and Related Compounds* (Eds: N. Garti, N. R. Widlak), AOCS Press, Urbana, IL **2012**, p. 151.
[16] A. Kitaigorodsky, *Molecular Crystals and Molecules*, Elsevier Science, Oxford **1973**.
[17] L. Bayés-García, T. Calvet, M. A. Cuevas-Diarte, S. Ueno, *Food Res. Int.* **2016**, *85*, 244.
[18] L. Bayés-García, T. Calvet, M. Àngel Cuevas-Diarte, S. Ueno, K. Sato, *CrystEngComm* **2013**, *15*, 302.
[19] L. Bayés-García, T. Calvet, M. À. Cuevas-Diarte, S. Ueno, K. Sato, *J. Phys. Chem. B* **2013**, *117*, 9170.
[20] L. Bayés-García, T. Calvet, M. À. Cuevas-Diarte, S. Ueno, K. Sato, *CrystEngComm* **2011**, *13*, 3592.
[21] R. I. Wille, E. S. Lutton, *J. Am. Chem. Soc.* **1966**, *43*, 491.
[22] A. S. Moorthy, R. Liu, G. Mazzanti, L. H. Wesdorp, A. G. Marangoni, *J. Am. Oil Chem. Soc.* **2017**, *94*, 187.
[23] L. H. Wesdorp, J. van Meeteren, S. de Jon, R. Giessen, P. Overbosch, P. Grootscholten, M. Struik, E. Royers, A. Don, T. de Loos, in *Structure and Properties of Fat Crystal Networks* (Eds: A. G. Marangoni, L. H. Wesdorp), CRC Press, Boca Raton, FL **2013**, p. 241.
[24] S. M. Ghazani, A. G. Marangoni, *Cryst. Growth Des.* **2018**, *18*, 4811.
[25] L. Bayés-García, T. Calvet, M. À. Cuevas-Diarte, S. Ueno, K. Sato, *J. Phys. Chem. B* **2015**, *119*, 4417.
[26] S. Ueno, A. Minato, H. Seto, Z. Amemiya, K. Sato, *J. Phys. Chem. B* **1997**, *101*, 6847.
[27] D. R. Kodali, D. Atkinson, D. M. Small, *J. Lipid Res.* **1990**, *31*, 1855.
[28] M. Baker, L. Bouzidi, N. Garti, S. S. Narine, *J. Am. Oil Chem. Soc.* **2014**, *91*, 559.
[29] M. R. Baker, L. Bouzidi, N. Garti, S. S. Narine, *J. Am. Oil Chem. Soc.* **2014**, *91*, 1685.
[30] M. Takeuchi, S. Ueno, K. Sato, *Food Res. Int.* **2002**, *35*, 919.
[31] L. Bouzidi, M. V. Boodhoo, T. Kutek, V. Filip, S. S. Narine, *Chem. Phys. Lipids* **2010**, *163*, 607.
[32] M. V. Boodhoo, T. Kutek, V. Filip, S. S. Narine, *Chem. Phys. Lipids* **2008**, *154*, 7.
[33] J. W. Hagemann, W. H. Tallent, *J. Am. Oil Chem. Soc.* **1972**, *49*, 118.
[34] C. Lu, B. Zhang, H. Zhang, Y. Guo, L. Dang, Z. Liu, Q. Shu, Z. Wang, *Ind. Eng. Chem. Res.* **2019**, *58*, 10044.
[35] P. Elisabettini, G. Lognay, A. Desmedt, C. Culot, N. Istasse, E. Deffense, F. Durant, *J. Am. Oil Chem. Soc.* **1998**, *75*, 285.
[36] A. van Langevelde, K. F. van Malssen, E. Sonneveld, R. Peschar, H. Schenk, *J. Am. Oil Chem. Soc.* **1999**, *76*, 603.
[37] A. J. van Langevelde, K. F. van Malssen, F. Hollander, R. Peschar, H. Schenk, *Acta Crystallogr., Sect. B: Struct. Sci., Cryst. Eng. Mater.* **1999**, *B55*, 114.
[38] J. B. van Mechelen, R. Peschar, H. Schenk, *Acta Crystallogr., Sect. B: Struct. Sci., Cryst. Eng. Mater.* **2008**, *B64*, 240.
[39] J. B. van Mechelen, R. Peschar, H. Schenk, *Acta Crystallogr., Sect. B: Struct. Sci., Cryst. Eng. Mater.* **2008**, *B64*, 249.
[40] J. B. van Mechelen, R. Peschar, H. Schenk, *Acta Crystallogr., Sect. B: Struct. Sci., Cryst. Eng. Mater.* **2006**, *B62*, 1131.
[41] J. B. van Mechelen, R. Peschar, H. Schenk, *Acta Crystallogr., Sect. B: Struct. Sci., Cryst. Eng. Mater.* **2006**, *B62*, 1121.
[42] A. van Langevelde, R. Peschar, H. Schenk, *Chem. Mater.* **2001**, *13*, 1089.
[43] D. R. Kodali, D. Atkinson, T. G. Redgrave, D. M. Small, *J. Lipid Res.* **1987**, *28*, 403.
[44] *Structure-Function Analysis of Edible Fats*, 2nd ed. (Ed: A. G. Marangoni), AOCS Press, Urbana, IL **2012**.
[45] K. Sato, M. Goto, J. Yano, K. Honda, D. R. Kodali, D. M. Small, *J. Lipid Res.* **2001**, *42*, 338.
[46] A. van Langevelde, K. F. van Malssen, R. Driessen, K. Goubitz, F. Hollander, R. Peschar, P. Zwart, H. Schenk, *Acta Crystallogr., Sect. B: Struct. Sci., Cryst. Eng. Mater.* **2000**, *B56*, 1103.
[47] K. Sato, in *Crystallization of Lipids: Fundamentals and Applications in Food, Cosmetics, and Pharmaceuticals* (Ed: K. Sato), John Wiley & Sons, New York **2018**, pp. 17–60.
[48] K. Sato, *Chem. Eng. Sci.* **2001**, *56*, 2255.
[49] S. de Jong, T. C. van Soest, *Acta Crystallogr., Sect. B: Struct. Sci., Cryst. Eng. Mater.* **1978**, *B34*, 1570.
[50] C. Himawan, V. M. Starov, A. Stapley, *Adv. Colloid Interface Sci.* **2006**, *122*, 3.
[51] H. M. Zacharis, *Chem. Phys. Lipids* **1977**, *18*, 221.
[52] J. Seilert, S. Rudolph, E. Flöter, unpublished.
[53] D. A. Pink, C. B. Hanna, C. Sandt, A. J. MacDonald, R. MacEachern, R. Corkery, D. Rousseau, *J. Chem. Phys.* **2010**, *132*, 54502.